Photosynthesis Research

Predicting light-induced stomatal movements based on the redox state of plastoquinone – theory and validation.

--Manuscript Draft--

Manuscript Number:	PRES-D-18-00130R3
Full Title:	Predicting light-induced stomatal movements based on the redox state of plastoquinone – theory and validation.
Article Type:	SI "The Modeling of Photosynthesis: Enzymes to Ecosystems"
Keywords:	stomatal conductance model; light response; plastoquinone; chlorophyll fluorescence; Gas exchange; ecosystem; crop models.
Corresponding Author:	Johannes Kromdijk University of Illinois at Urbana-Champaign UNITED STATES
Corresponding Author Secondary Information:	
Corresponding Author's Institution:	University of Illinois at Urbana-Champaign
Corresponding Author's Secondary Institution:	
First Author:	Johannes Kromdijk
First Author Secondary Information:	
Order of Authors:	Johannes Kromdijk
	Katarzyna Głowacka
	Stephen P Long
Order of Authors Secondary Information:	
Author Comments:	Comments by Nerea Ubierna have now also been incorporated.
Abstract:	Prediction of stomatal conductance is a key element to relate and scale up leaf-level gas exchange processes to canopy, ecosystem and land surface models. The deterministic models that are typically employed for this purpose are simple and elegant formulations which relate stomatal conductance on a leaf area basis to the net rate of CO2 assimilation, humidity and CO2 concentration. Although light intensity is not directly modelled as a stomatal opening cue, it is well known that stomata respond strongly to light in at least two independent ways. Stomatal opening is strongly stimulated by irradiance with blue light and stomata also respond to light intensity in a way that is often termed the 'red light' response. The direct relationship of CO2 assimilation to stomatal conductance in deterministic models can thus be seen as a combined representation of the 'red light' and 'blue light' responses of stomatal conductance. Here, we present a modified deterministic stomatal conductance model explicitly accounting for the stomatal red light response, based on a putative plastoquinone redox state signal. The modified model showed similar prediction accuracy compared to models using a relationship between stomatal conductance and net assimilation rate. However, fitted parameter values with the modified model varied much less across different measurement conditions, lessening the need for frequent re-parameterization to different conditions required of the current model and allowing for more robust predictions under future climate conditions. We also present a simple and easy to parameterize extension to the widely used Farquhar-Von Caemmerer-Berry photosynthesis model to facilitate coupling with the modified stomatal conductance model.
Response to Reviewers:	final comments by reviewers had already been incorporated
Additional Information:	
Question	**Response**

Contribution to Special Issue Photosynthesis research: Improvements and advances in modeling photosynthetic processes

Title: Predicting light-induced stomatal movements based on the redox state of plastoquinone – theory and validation.

Authors: Johannes Kromdijk[1,2,6], Katarzyna Głowacka[1,3,5], Stephen P. Long[1,4]

Affiliations:

[1]Carl R. Woese Institute for Genomic Biology, University of Illinois at Urbana-Champaign, 1206 West Gregory drive, IL61801, Urbana, Illinois, USA.

[2]Department of Plant Sciences, University of Cambridge, Downing site, CB23EA, Cambridge, United Kingdom.

[3]Institute of Plant Genetics, Polish Academy of Sciences, 60-479 Poznań, Poland

[4]Lancaster Environment Centre, University of Lancaster, LA1 1YX, UK

[5]Current address: Department of Biochemistry, University of Nebraska-Lincoln, N246 Beadle Center, 1901 Vine Street, Lincoln, Nebraska, USA.

[6]Corresponding author: jk417@cam.ac.uk

Abstract

Prediction of stomatal conductance is a key element to relate and scale up leaf-level gas exchange processes to canopy, ecosystem and land surface models. The empirical models that are typically employed for this purpose are simple and elegant formulations which relate stomatal conductance on a leaf area basis to the net rate of CO_2 assimilation, humidity and CO_2 concentration. Although light intensity is not directly modelled as a stomatal opening cue, it is well known that stomata respond strongly to light. One response mode depends specifically on the blue light part of the light spectrum, whereas the quantitative or 'red' light response is less spectrally defined and relies more on the quantity of incident light. Here, we present a modification of an empirical stomatal conductance model which explicitly accounts for the stomatal red light response, based on a mesophyll-derived signal putatively initiated by the chloroplastic plastoquinone redox state. The modified model showed similar prediction accuracy compared to models using a relationship between stomatal conductance and net assimilation rate. However, fitted parameter values with the modified model varied much less across different measurement conditions, lessening the need for frequent re-parameterization to different conditions required of the current model. We also present a simple and easy to parameterize extension to the widely used Farquhar-Von Caemmerer-Berry photosynthesis model to facilitate coupling with the modified stomatal conductance model, which should enable use of the new stomatal conductance model to simulate ecosystem water vapour exchange in terrestrial biosphere models.

Keywords: stomatal conductance model; light response; plastoquinone; chlorophyll fluorescence; gas exchange; crop models

Introduction

Terrestrial plants need to take up water from the surrounding environment, retain or transfer water internally, as well as acquire carbon dioxide from the surrounding air to drive photosynthetic carbon assimilation. This trade-off between optimizing carbon uptake via atmospheric diffusion versus minimizing water loss to the atmosphere drove the evolution of highly specialized, controllable stomatal pores in the epidermis of plant leaves (Chater et al. 2017). Stomatal pores are flanked by a pair of guard cells, the only photosynthetic cells of the epidermis, in which turgor changes regulate the pore's aperture in response to a variety of cues (Kollist et al. 2014), such as leaf (and plant) water status (Mott and Parkhurst 1991; Whitehead 1998), carbon dioxide concentration (Engineer et al. 2016) and light (Assman and Shimazaki 1999; Kaiser and Kappen 1997). The importance of the control of stomatal aperture for plant fitness is clear. Stomatal conductance to water vapour strongly determines transpiratory water loss at leaf-level (Pearcy et al. 1989) and this relationship can be scaled to canopy transpiration, when accounting for leaf area, canopy conductance and degree of coupling between the canopy and atmosphere (e.g. Mielke et al. 1999). In doing so, it can be shown that stomatal movements significantly influence ecosystem water (and energy) exchange (Wehr et al. 2017). In fact, recent estimates show that transpiratory water loss through stomata accounts for 43% to 75% of global terrestrial evapotranspiration (Wei et al. 2017). This importance of stomatal conductance as a control factor for gaseous fluxes across spatial scales emphasizes the need for robust stomatal conductance models to accurately simulate changes in response to - and interactions with - the surrounding environment in current and future climate scenarios.

A wide variety of models for stomatal conductance exist, ranging from very detailed to more simplified descriptions (for reviews, see Buckley 2017; Damour et al. 2010). The majority of stomatal conductance models cover only steady state responses, although significant progress is being made to capture dynamic behavior of stomatal conductance (Bellasio et al. 2017; Vialet-Chabrand et al. 2017; Wang et al. 2017). Despite these advances, the empirical Ball-Woodrow-Berry (BWB) model (Ball et al. 1986) is still the

most widely used prediction tool for stomatal conductance in models extending across spatial scales. The BWB model is a very simple, elegant formulation, which relates (steady state) stomatal conductance to the humidity and CO_2 concentration of air surrounding the leaf, and the prevailing rate of photosynthesis, using slope (g_1) and intercept (g_0) parameters. The simplicity of the BWB model facilitates easy coupling to the Farquhar-Von Caemmerer-Berry (FvCB) photosynthesis model (Farquhar et al. 1980), which has been convenient for use in leaf and canopy gas exchange models, as well as ecosystem and land surface models for climate simulation (Bonan et al. 2014).

The original BWB model considers humidity as a percentage of saturated vapour pressure, but this has been altered in several modified versions to a parameter based on vapour pressure deficit (e.g. Dougherty et al. 1994; Leuning 1995; Medlyn et al. 2011). Additional dependencies on soil moisture, plant water status and abscisic acid concentration (Tenhunen et al. 1990; Wang and Leuning 1998, Gutschick and Simonneau 2002) can also be added. The effects of CO_2 on stomatal movements are directly accounted for via multiplication with the inverse of ambient CO_2 concentration, as well as via an implicit feedback through multiplication with net CO_2 assimilation rate (A_n), which is itself responsive to CO_2 concentration. The influence of light on stomatal movements is not explicitly accounted for in the BWB model, but is implicitly assumed to be equal to the effects of light on A_n, thus assuming a direct link between photosynthesis and light-induced stomatal movements. Whereas this assumption is a convenient approximation, it is not consistent with current understanding of light-induced stomatal movements. Instead, light affects stomatal movements in at least two separate ways. Firstly, illumination with (low intensity) blue light activates phototropins, blue light photoreceptors, which in turn activate a signal transduction chain leading to stomatal opening (Inoue and Kinoshita 2017). These blue light effects can be most clearly observed in the background of red-light illumination, which also stimulates stomatal opening. However, whereas several signalling components of the blue-light response of stomatal opening have been elucidated, the ‘quantitative’ or ‘red light’ response of stomatal conductance is less well understood. Some evidence suggests that phytochromes A and B, red:far-red light photoreceptors, might

be involved (Wang et al. 2010) as well as a specific set of MYB transcription factors (*At*MYB60 and *At*MYB61, Liang et al. 2005). Additionally, whereas the blue-light response appears entirely located in the guard cells, the red-light response seems to depend on a mesophyll-derived signal (Mott et al. 2008; Lawson et al. 2014). This signal was long assumed to be directly related to photosynthesis, but stomatal conductance in plants with transgenically decreased photosynthetic capacity was not decreased proportionally (e.g. Von Caemmerer et al. 2004, Baroli et al. 2008; Lawson et al. 2008), providing evidence that the mesophyll signal does not scale directly with photosynthetic rates. Additionally, responses to red-light cannot simply be explained by concomitant effects on intercellular CO_2 concentration (C_i), since stomata still respond to red light when C_i is kept constant (Messinger et al. 2006). Busch (2014) suggested that instead of a photosynthesis-derived signal, the redox state of the chloroplastic plastoquinone (*PQ*) pool might be signalled to the stomatal guard cells. Consistent with this hypothesis, we recently observed tightly and linearly coordinated changes in the redox state of quinone A, estimated by fluorescence parameter $1 - q_L$ (Kramer et al. 2004) and stomatal conductance in tobacco with modified levels of photosystem II subunit S (PsbS) (Głowacka et al. 2018), which is a strong determinant of the amplitude of non-photochemical quenching and therefore also affects the redox state of the chloroplastic electron transport chain.

In the current manuscript we present a modified stomatal conductance model, which explicitly accounts for these observed responses. The parameterization of the resulting model is demonstrated to be less sensitive to measurement conditions compared to the BWB models which simulate stomatal conductance as a function of net assimilation rate. We also show that a simple extension to the FvCB photosynthesis model can be used to predict $1 - q_L$ from combined gas exchange and chlorophyll fluorescence measurements, which facilitates coupling to the modified stomatal conductance model.

Materials and Methods

Modified stomatal conductance model

The BWB model (Ball et al. 1986) calculates stomatal conductance to water vapour from a linear product of net assimilation rate A_n, relative humidity h_s and the inverse of CO_2 concentration surrounding the leaf (C_a). Here we use the recent version by Medlyn et al. (2011) as a starting point, where the inverse square-root of atmospheric vapour-pressure-deficit (VPD_A) is used instead of h_s to capture effects of humidity on g_s. The resulting term is scaled empirically to measured stomatal conductance, using a slope parameter g_1 and intercept parameter g_0, such as shown in Eq. 1.

$$g_s = g_0 + 1.6 \cdot \left(1 + \frac{g_1}{\sqrt{VPD_A}}\right) \cdot \frac{A_n}{C_a} \qquad \text{Eq. 1}$$

Recent data (Głowacka et al. 2018) suggest that the stomatal 'quantitative' or 'red' light response may be initiated by a *PQ* redox signal, which we approximate by $1 - q_L$ i.e. the redox state of the quinone bound to the Q_A site at photosystem II (PSII). We therefore replaced A_n in Eq. 1 with $(1 - q_L)$ (Eq. 2). Note that the empirical constants in Eq. 1 are used similarly to Eq. 2 but have been renamed, to facilitate easy comparison between parameter estimation based on the Medlyn model and the modified model.

$$g_s = g_{0,new} + 1.6 \cdot \left(1 + \frac{g_{1,new}}{\sqrt{VPD_A}}\right) \cdot \frac{1 - qL}{C_a} \qquad \text{Eq. 2}$$

Extension of the FvCB photosynthesis model to simulate q_L

The biochemical model for leaf photosynthesis by Farquhar et al. (1980; abbreviated as FvCB model) is widely used in conjunction with stomatal models such as Eq. 1. Coupling between the FvCB model and the new stomatal conductance model in Eq. 2 would require simulation of q_L. Therefore, we present a simple extension of the FvCB model to allow simulation of q_L. The FvCB model has a switch-point structure and simulates net assimilation rate as the minimum of three limiting factors: RuBP carboxylation-limited rate (A_c), RuBP regeneration-limited rate (A_j) and triose-phosphate utilization limited rate (A_{TPU}).

$$A_c = \frac{V_{cmax}\cdot(C_c-\Gamma^*)}{C_c+K_c\cdot(1+\frac{O_c}{K_o})} - R_d \quad \text{Eq. 3a}$$

$$A_j = \frac{J\cdot(C_c-\Gamma^*)}{4C_c+8\Gamma^*} - R_d \quad \text{Eq. 3b}$$

$$A_{TPU} = 3V_{TPU} - R_d \quad \text{Eq. 3c}$$

$$A_n = \min(A_c, A_j, A_{TPU}) \quad \text{Eq. 3d}$$

Here, V_{cmax} is the maximal rate of RuBP carboxylation and K_c and K_o are the Michaelis-Menten constants to describe CO_2 and O_2 effects on RuBP carboxylation. C_c represents the chloroplastic CO_2 concentration, Γ^* represents the CO_2 compensation point in the absence of R_d, and R_d represents mitochondrial respiration not associated with photorespiration. V_{TPU} is the maximal rate of triose phosphate utilization and O_c represents the O_2 concentration in the chloroplast, which was assumed to equal ambient.

Next, the rate of whole-chain electron transport (J; Eq. 4) was modelled as a function of absorbed light intensity (PFD_{abs}) using a non-rectangular hyperbola, with initial slope α, asymptote J_{max} and shape factor θ.

$$J = \frac{\alpha\cdot f_{PSII}\cdot PFD_{abs}+J_{max}-\sqrt{(\alpha\cdot f_{PSII}\cdot PFD_{abs})^2-4\cdot\theta\cdot\alpha\cdot f_{PSII}\cdot PFD_{abs}+J_{max}}}{2\cdot\theta} \quad \text{Eq. 4}$$

Here, f_{PSII} represents the proportion of absorbed light partitioned to PSII. The level of J was used to calculate the operating efficiency of photosystem II (Φ_{PSII}) at a given light level:

$$\Phi_{PSII} = \frac{J}{PFD_{abs}\cdot f_{PSII}} \quad \text{Eq. 5}$$

To describe the steady state level of non-photochemical quenching (NPQ) as a function of light intensity (PFD), a sigmoidal Hill-function was used (Eq. 6a), with basal level NPQ_0, light intensity at half amplitude (K_{NPQ}), hill coefficient ($nNPQ$) and asymptote (NPQ_{max}). The level of NPQ at the $PFD = 0$ limit was assumed to equal zero (Eq. 6b).

$$PFD > 0 \rightarrow NPQ = \frac{NPQ_{max} - NPQ_0}{\left(\left(\frac{K_{NPQ}}{PFD_{abs}}\right)^{nNPQ} + 1\right)} + NPQ_0 \quad \text{Eq. 6a}$$

$$PFD = 0 \rightarrow NPQ = 0 \quad \text{Eq. 6b}$$

Maximal fluorescence without dark-adaptation at a given light level (F_m') was calculated using *NPQ* (from Eq. 6) and dark-adapted maximal fluorescence F_m according to Eq. 7. The corresponding level of *F'* was computed with Eq. 8, using Φ_{PSII} from Eq. 5:

$$F'_m = \frac{F_m}{NPQ+1} \quad \text{Eq. 7}$$

$$F' = \frac{F_{m'}}{1-\Phi_{PSII}} \quad \text{Eq. 8}$$

To predict minimal fluorescence without dark-adaptation (F_o') as a function of light intensity, we separately considered effects of suppression of fluorescence via *NPQ* and elevation of fluorescence due to photo-inactivated reaction centers. The decrease in F_o' relative to F_o as a result of *NPQ* (calculated as $F_o{'}_{NPQ}$) was estimated from F_m' and F_o according to Oxborough and Baker (1997):

$$F_o{'}_{NPQ} = \frac{F_o}{\frac{F_v}{F_m} + \frac{F_o}{F_{m'}}} \quad \text{Eq. 9}$$

Using $F_o{'}_{NPQ}$ from Eq. 9, the effects of *NPQ* on the maximal PSII quantum efficiency in the light ($\frac{F_{v'}}{F_{m'}}$) can be predicted:

$$\left(\frac{F_{v'}}{F_{m'}}\right)_{NPQ} = 1 - \frac{F_o{'}_{NPQ}}{F_{m'}} \quad \text{Eq. 10}$$

Next, we used an empirical relationship to predict the elevation of minimal fluorescence due to inactivation of reaction centers. Hendrickson et al. (2005) showed that the energy flux approximated by $0.5 \cdot PFD_{abs} \cdot \frac{F'}{F_{m'}}$ is a reasonable estimator of the rate constant of photo-inactivation. Therefore, we

predicted the relative difference between $(\frac{F_v'}{F_m'})_{NPQ}$ from Eq. 10 and observed $\frac{F_v'}{F_m'}$ by a linear function of $0.5 \cdot PFD_{abs} \cdot \frac{F'}{F_m'}$according to Eq. 11:

$$1 - \frac{\left(\frac{F_v'}{F_m'}\right)}{\left(\frac{F_v'}{F_m'}\right)_{NPQ}} = m \cdot \left(0.5 \cdot PFD_{abs} \cdot \frac{F'}{F_m'}\right) + n \quad \text{Eq. 11}$$

The empirical coefficients *m* and *n* were fitted on light response curves of chlorophyll fluorescence parameters. Combining Eq. 11 with simulated fluorescence levels from Eq. 7 and 8 then allowed calculation of q_L using the formulation by Kramer et al. (2004):

$$q_L = \frac{F_m' - F'}{F_m' - F_o'} \cdot \frac{F_o'}{F'} \quad \text{Eq. 12}$$

Coupling the photosynthesis and stomatal conductance models

Using the equations presented above, q_L can be calculated, which provides a handle for coupling the photosynthesis model with the modified stomatal conductance model. First of all, the intercellular CO_2 concentration C_i is dependent on the CO_2 concentration in the chloroplast C_c at a given rate of photosynthesis. The value of C_i could therefore be modelled based on the photosynthesis model using Fick's law of diffusion (Eq. 13).

$$C_i = C_c + \frac{A_n}{g_m \cdot P} \quad \text{Eq. 13}$$

Here, *P* represents atmospheric pressure and g_m is mesophyll conductance to CO_2. Additionally, C_i can be predicted from the CO_2 concentration surrounding the leaf (C_a), the rate of A_n, and the value of stomatal conductance (g_s) from Eq. 1 or 2.

$$C_i = \frac{\left(\frac{1}{\frac{1.6}{g_s} + \frac{1.37}{g_{bl}} - \frac{VPD_L}{2 \cdot P \cdot \left(\frac{1}{g_s} + \frac{1}{g_{bl}}\right)}}\right) \cdot C_a - A_n}{\left(\frac{1}{\frac{1.6}{g_s} + \frac{1.37}{g_{bl}} + \frac{VPD_L}{2 \cdot P \cdot \left(\frac{1}{g_s} + \frac{1}{g_{bl}}\right)}}\right)} \quad \text{Eq. 14}$$

Here, g_{bl} represents the conductance to H_2O through the leaf boundary layer, VPD_L represents leaf-to-air vapor pressure deficit. Using these two formulations for C_i, the models were coupled by iterative minimization of differences between Eq.13 and 14.

Parameter estimation for the Medlyn model and modified stomatal conductance model

The parameters for the stomatal conductance models were estimated using measurements on tobacco plants. Tobacco seeds (*Nicotiana tabacum*, cv 'Petite Havana') were germinated on soilless cultivation medium (LC1 Sunshine mix, Sun Gro Horticulture, Agawam, MA, USA) in a controlled environment walk-in growing chamber (Environmental Growth Chambers, Chagrin Falls, OH, USA) with photoperiod set to twelve hours and temperature controlled at 25 °C / 23 °C (day/night). Five days after germination seedlings were moved to the greenhouse, transplanted to 9 × 4 potting trays (3600 series, Hummert International, Earth City, MO, USA) and grown until two true leaves had emerged. When two true leaves had emerged, seedlings were transplanted to 3.8 L pots (400C, Hummert International, Earth City, MO, USA) filled with growing medium (LC1 Sunshine mix, Sun Gro Horticulture) supplemented with 10 g granulated fertilizer per pot (Osmocote Plus 15/9/12, The Scotts Company LLC, Marysville, OH, USA). Pots were spaced 30 cm apart on greenhouse tables and watered and positions randomized every two days.

Gas exchange measurements were performed on the youngest fully expanded leaf after 2.5 weeks of growth (leaf 5), using an open gas exchange system (LI6400XT, LI-COR, Lincoln, Nebraska, USA) equipped with a 2 cm^2 leaf chamber fluorometer (LCF6400-40, LI-COR), corrected for diffusive leaks between cuvette and the surrounding atmosphere. Two sets of light response curves of photosynthesis, fluorescence and stomatal conductance were used to parameterize the Medlyn and modified stomatal conductance models (see Fig. S1). Leaves were dark-adapted and clamped in the gas exchange cuvette, with block temperature controlled at 25 °C. After measuring F_o and F_m chlorophyll fluorescence levels, light intensity was increased stepwise from 0 to 50, 80, 110, 140, 170, 200, 300, 400, 500, 600, 800, 1000, 1500 and 2000 μmol m^{-2} s^{-1}. When steady state was achieved (typically at least 15 min waiting time per

step), gas exchange parameters were logged and F' and F_m' were determined using the multiphase flash routine (Loriaux et al. 2013). Additionally, F_o' was measured by switching the actinic light off briefly while turning on far-red LEDs (λ_{max} = 740 nm) to rapidly re-oxidize quinone A. The chlorophyll fluorescence levels at each light intensity were used to compute q_L according to Eq. 12. For the first set of light response curves, CO_2 concentration inside the cuvette was controlled at 380 µmol mol^{-1} and the light intensities were achieved solely with red light emitting diodes (λ_{max} = 630 nm). This set has been previously published in Głowacka et al. (2018). For set 2, CO_2 concentration in the reference air was controlled at 1000 µmol mol^{-1} and light intensities were a sum of 90% red and 10% blue (λ_{max} = 470 nm) on a photon flux basis. The curves were performed on n = 6 biological replicates for set 1 and n = 7 for set 2. These measurements resulted in two sets of g_s, A_n and 1 - q_L, which were used to estimate parameters g_0 and g_1 in Eq. 1 as well as $g_{0,new}$ and $g_{1,new}$ in Eq. 2 via linear regression.

Parameter estimation for the photosynthesis model

Parameter estimation of the photosynthesis model required measuring the capacity for leaf photosynthetic biochemistry (see Fig. S1). For this purpose, CO_2 response curves of photosynthesis were performed on the youngest fully expanded leaf (n = 6 biological replicates). Leaves were clamped in the gas exchange cuvette with light intensity set to 2000 µmol m^{-2} s^{-1} (10% blue). CO_2 concentration in the airstream was controlled to 400 µmol mol^{-1}, and block temperature set to 25 °C. After steady state had been achieved, CO_2 was varied from 400 to 300, 200, 100, 75, 400, 400, 500, 600, 700, 800, 1200, 1600 and 1900 µmol mol^{-1}. At each CO_2 concentration, gas exchange values were logged, when the coefficient of variation in net leaf CO_2 uptake rate (A_n) and intercellular CO_2 concentration (C_i) averaged over 10 s became less than 1% (minimum wait time 1 min, maximum wait time 4 min). V_{cmax} and V_{TPU} were obtained by fitting the photosynthesis model according to Sharkey et al. (2007) and temperature corrections within. Mesophyll conductance (g_m) was not co-fitted but a value of 0.60 mol m^{-2} s^{-1} bar^{-1} at 25 °C was derived separately on a parallel set of tobacco plants, using carbon isotope discrimination measurements in parallel with gas exchange from cryogenic trapping and isotope ratio mass spectrometry as described in Kromdijk et al.

(2010) and model equations outlined in Evans and Von Caemmerer (2013). R_d was estimated as the y-intercept from the linear regression of A_n versus J at low light (Yin et al. 2009), where J was obtained from the light response curves as described above. To convert incident to absorbed photon flux in both sets of curves, light absorptance was measured on the same leaf position where gas exchange analysis had also been performed, using an integrating sphere (LI1800, LI-COR) connected to a spectrometer (USB-2000, Ocean Optics Inc, Dunedin, Florida, USA). Incident photon flux was converted to absorbed photon flux (PFD_{abs}) using the measured absorptance at the actinic wavelengths used.

Using the coupled model to predict field observations of A_n and g_s

Survey-style measurements on field-grown tobacco were performed on a bright, hot day (July 21, 2015) at the University of Illinois farm in Urbana (40.11°N, 88.21°W). Early morning measurements had to be delayed until all morning dew of the leaves had evaporated, which occurred around 08:00. Thus, measurements were started at 08:15 and repeated every 90 minutes until 20:15, just prior to sunset. At each time-point, ambient light intensity was first measured using the external PAR-sensor of the LI6400XT. Subsequently, light intensity in the cuvette was set to equal the ambient intensity (using 90% red and 10% blue), block temperature was set to measured air temperature and CO_2 concentration in the airstream was set to 400 μmol mol^{-1}. Leaves were clamped in the cuvette and gas exchange values were logged as soon as stomatal conductance reached steady rates for 10 s (based on visual assessment of the strip-charts), which happened typically after 1.5 to 2 minutes. Parameter estimation for the photosynthesis model was performed using additional CO_2 and light response curves measured on the field-grown plants. The coupled model was used to predict stomatal conductance based on the parameter estimates for g_0, g_1, $g_{0,new}$ and $g_{1,new}$ from the plants grown under controlled conditions, as well as using re-calibrated parameter values from a best fit with observations.

Implementation and model fitting

The equations were implemented in Matlab (Version 8.1.0.604, R2013a, The Mathworks Inc. Natick, MA, USA). Parameter estimation of the stomatal conductance and photosynthesis models was performed using constrained nonlinear minimization ('fmincon' algorithm with global search) of least squares differences. Linear regressions were performed with SigmaPlot (Version 14.0, SYSTAT Software Inc., San Jose, California, USA). Re-calibration of the stomatal conductance model under field conditions was performed by minimizing residuals using a grid-search for g_0, g_1, $g_{0,new}$ or $g_{1,new}$.

Results

Stomatal conductance model

The measured light responses of stomatal conductance showed highly significant linear correlations with both A_n and $1 - q_L$ ($P < 0.005$, Fig. 1A and B). The slopes of the regressions were significantly different between the two sets of light response curves (Student's t-test, $P < 0.05$), as could be expected from the well-known suppression effect of high CO_2 on stomatal movements. The slope of both stomatal conductance models is essentially a linear multiplication of response factors (i.e. $A_n \times C_a^{-1} \times VPD_A^{-0.5}$ or $(1 - q_L) \times C_a^{-1} \times VPD_A^{-0.5}$). Therefore, the ratio of the slopes of the regressions of g_s against either A_n or $1 - q_L$ should equal $(C_a^{-1}{}_{set1} \times VPD_A^{-0.5}{}_{set1}) / (C_a^{-1}{}_{set2} \times VPD_A^{-0.5}{}_{set2})$, which was calculated to be 2.27. The measured slope ratio between the linear regressions in Fig. 1A (A_n vs g_s) was 4.67, whereas the regressions in Fig. 1B ($1 - q_L$ vs g_s) showed a slope ratio of 3.06, which was considerably closer to the predicted value. This suggests that the relationship between g_s and $1 - q_L$ is more conserved than between g_s and A_n when measurement conditions are varied. This was also confirmed by fitting the model parameters g_0 and g_1 (Fig. 2A and C) or $g_{0,new}$ and $g_{1,new}$ (Fig. 2B and D) for each individual light response curve. One light response curve in set 2 did not converge to a reasonable estimate for g_1 in the Medlyn model, and was discarded to avoid confounding the comparison between A_n and $1 - q_L$. For the remaining 12 light response curves, variation in stomatal conductance was adequately captured by both models. However, whereas the fitted slope parameter g_1 decreased significantly by 58% for measurements at 1000 µmol mol^{-1} CO_2 and 10% blue compared to 380 µmol mol^{-1} CO_2 and 100% red light (1.90 ± 0.25 vs 0.60 ± 0.15, P = 0.001, Fig. 3A), fitted $g_{1,new}$ did not vary significantly (103 ± 8 vs 84 ± 8, P = 0.10, Fig. 3B).

Predicting q_L with the extended photosynthesis model

To facilitate the integration of $1 - q_L$ as a predictor of light-induced stomatal movements in higher level models, we extended the widely used FvCB biochemical model for leaf photosynthesis (Farquhar et al. 1980) to allow simulation of q_L. First, leaf biochemical capacity for RuBP carboxylation (V_{cmax}) and triose

phosphate utilization (V_{TPU}) were estimated based on CO_2 response curves (Fig. 4A). Light response curves were used to parameterize descriptive equations for whole-chain electron transport rate *J* (Fig. 4B) and non-photochemical quenching *NPQ* (Fig. 4C) and estimate the rate of mitochondrial respiration in the light (R_d) as the y-intercept of the initial linear response of A_n to *J* (Fig. 4D). All parameter estimates are shown in Table 1. These estimates were then used to simulate fluorescence parameters F_m', F' and F_o' (Fig. 5A-C). Simulation of F_o' showed a slight mismatch compared to the measured values at low light intensity, which is due to the fact that the relationship described in Eq. 17 becomes slightly curvi-linear at low light. However, the overall fit between measured and simulated fluorescence parameters was adequate to accurately reproduce most of the observed variation in q_L ($R^2 = 0.984$) and the linear correlation did not differ significantly from x = y ($P > 0.05$, Fig. 6A and B).

Coupled model for photosynthesis and stomatal conductance

Simulation of q_L through the extended photosynthesis model shown in Fig. 6 provided a coupling point for the modified stomatal conductance model. The coupled stomatal conductance – photosynthesis model was used to simulate A_n (Fig. 7A) and g_s (Fig. 7B) as a function of light intensity by iteratively solving differences between the two equations for intercellular CO_2 concentration C_i (Eq. 18 and 19). Both were simulated reasonably accurately across the light response, although a slight mismatch in the curvature of g_s was observed (Fig. 7B).

As an independent verification, diurnal gas exchange measurements on field-grown tobacco were used to further test the performance of the coupled model. Measurements were performed on a well-watered tobacco crop on a hot, clear day in mid-summer (Fig. 8A). The first measurement point was taken at 08.15, when light intensity had already reached 700 μmol m^{-2} s^{-1} and A_n and g_s were already quite high (averaging 20.0 μmol m^{-2} s^{-1} and 0.55 mol m^{-2} s^{-1}, respectively). Subsequent measurements showed a slight increase in g_s towards 11.15 followed by a gradual decline throughout the afternoon. A_n also increased towards mid-day, reaching maximum values somewhat later than g_s, at 12:45 and 14:15, followed by a gradual decline throughout the remainder of the photoperiod.

To simulate these observations, we used both stomatal conductance models with either the parameter estimation from plants grown under controlled conditions or re-calibrated on the field-grown plants, while the photosynthesis model was parameterized on the field-grown plants at all simulations. Using the parameter estimates from controlled conditions for either the Medlyn or modified stomatal conductance model resulted in severe underestimation of stomatal conductance and net assimilation rate (Fig. 8B and C) as could be expected based on known differences in stomatal acclimation between controlled versus field conditions. A better match between modelled and observed data was obtained by re-calibration of the stomatal conductance model by minimizing the residuals between modelled and observed g_s. Model predictions with re-calibrated parameters showed a reasonable match with observed A_n and g_s for the majority of the time-points except for late in the photoperiod (17:15 and 18:45), where A_n and g_s were lower than predicted by the model. The minimized residuals were marginally smaller for the modified model compared to the Medlyn model, (0.115 vs 0.123). In addition, the residuals across a wide range of parameter values remained considerably lower in the modified stomatal conductance model, compared to the Medlyn model (0.115-0.162 vs 0.123-0.210 for parameter values shown in Fig. S2).

Discussion

Modelling light-induced stomatal movements

Models for stomatal conductance are important components of ecosystem, land surface and even earth system models in predicting future climate and biosphere productivity. Here we have shown that the widely used empirical BWB model for stomatal conductance (version by Medlyn *et al.* 2011) can be changed to incorporate the putative causal relationship between *PQ* redox state and light-induced stomatal movements (Busch 2014; Głowacka et al. 2018) yet kept simple enough to facilitate easy integration in models of greater scale. The modification was shown to lead to more conserved estimates for the slope parameter $g_{1,new}$ across different measurement conditions, which should help to increase confidence in predictions under future climates. The modifications to the model arguably represent a more mechanistic basis for stomatal responses to light, compared to the Medlyn model, although it is still very empirical and simplistic. Whereas more mechanistic models can typically be expected to do a better job in generating new insights and predicting g_s outside the validated range (Buckley 2017), they have a tendency to become too complex or include difficult to estimate parameters, which can make inclusion in levels of greater scales tricky. Therefore, there is still a need to refine empirical models such as presented here.

Although tobacco guard cells are known to respond only very weakly to the addition of blue light (Marten et al. 2008), it is possible that the slope parameters g_1 and $g_{1,new}$ may not strictly represent only the quantitative stomatal 'red' light response for the second set of response curves. Further testing in different species will need to be done to verify this. Interestingly, the over-excitation of photosystem II compared to photosystem I by blue light may directly promote a more reduced *PQ* redox state, which is hypothesized to lead to stomatal opening (Busch 2014, Glowacka et al. 2018). If so, the putative causal relationship between $1 - q_L$ and g_s implies that the stronger response of stomatal conductance to blue light may also arise via the 'red light' response, i.e. without the phototropin signaling cascade, although this

effect would be more apparent at higher ratios between red and blue light than 9 to 1 used here and would also depend on parallel effects on induction of *NPQ*.

Estimation of *NPQ* and q_L

To couple the new model of g_s based on $1 - q_L$ with other models, requires accurate prediction of q_L. We have presented a simple extension to the widely used FvCB model for photosynthesis (Farquhar et al. 1980), which is easy to parameterize and can be used to predict q_L reasonably well across a range of light intensities (Fig. 6). To circumvent the need for dark measurements for F_o', we simulated non-photochemical quenching and photo-inactivation effects on F_o. For non-photochemical quenching effects we used the formulation for F_o' by Oxborough and Baker (1997), which simulates the decrease in F_o' based on the decrease in F_m' relative to F_m. The fluorescence increase due to photo-inactivation was simulated by an empirical relationship with the estimated energy flux through non-photochemical dissipation pathways (fluorescence, as well as regulated and constitutive thermal dissipation), which has been shown to be linearly correlated with the rate coefficient of photo-inactivation of PSII reaction centers (Hendrickson et al. 2005). This relationship was calibrated on the differences between $F_o'_{NPQ}$ and measured F_o' (by turning off actinic light and application of weak far-red illumination) under controlled conditions, which confirmed a strong linear relationship, except for very low PFD where the relationship tended to be slightly curvilinear.

The model simulations of q_L further depend on accurate estimation of *NPQ*. We chose to use an empirical sigmoidal Hill function, which was sufficient to demonstrate the use of $1 - q_L$ as a predictor of light-induced stomatal movements, but carries limited biological meaning. Additionally, treatment of *NPQ* as an independent parameter does not take account of the intimate connection between photosynthesis and thermal dissipation of absorbed light energy in the photosynthetic antenna complexes. The presented approach may therefore be improved by linking the description of *NPQ* by Eq. 6 to the parameters describing photosynthetic capacity such as V_{cmax} and J_{max}, or using altogether more mechanistic models for simulation of photosynthesis and non-photochemical quenching (e.g. Zaks et al. 2012, Morales et al.

2018). Interestingly, the estimation of *NPQ* at larger scales has gained a lot of interest recently due to development of gross primary productivity (GPP) proxies based on ground-based or remotely sensed measurements of solar induced fluorescence (SIF, reviewed by Porcar-Castell et al. (2014) and several others). Here, the interaction between steady state photosynthesis and the passive emission of chlorophyll fluorescence provides an optical signal which can be used to estimate GPP. However, since steady state fluorescence is the product of absorbed light and the quantum yield of fluorescence, both photochemical and non-photochemical quenching can affect the SIF signal. Hence, additional modelling or parallel proxies for *NPQ* are required in order to use SIF signals as a proxy for GPP. One often-used proxy for *NPQ* is the photochemical reflectance index (PRI, Gamon et al. 1992), which is based on the broadband scattering change at 531 nm associated with pigment conversions in the xanthophyll cycle and a conformational change in the PSII antenna, which accompanies energy-dependent quenching (Bilger and Bjorkman 1994; Johnson et al. 2009). Short-term (diurnal) variations in the PRI signal can be successfully used to provide a proxy for canopy or ecosystem light use efficiency (Gamon et al. 1997; Hilker et al. 2011). Our demonstration that $1 - q_L$ can be used as a proxy for light-induced stomatal movements suggests that in addition to light use efficiency, optical proxies such as PRI may also turn out to be useful in constraining ecosystem water vapour exchange estimates based on stomatal conductance in terrestrial biosphere models.

More robust estimation of g_s across different conditions

We have demonstrated that using the fluorescence parameter $1 - q_L$ instead of A_n makes the slope parameter in the stomatal conductance model (g_1 and $g_{1,new}$) more robust against differing measurement conditions (Fig. 3). In addition, residuals of the modified stomatal conductance model were consistently lower than for the Medlyn model across a wide range of parameter values (Fig. S2). This is of great value to increase confidence in predictions of vegetation responses to future climate conditions. Slope and intercept parameters of BWB model (Ball et al. 1986) and the derivation by Medlyn et al. (2011) have been reported to vary substantially between species, and species-specific parameterization greatly

improved model predictions of A_n and g_s (Wolz et al. 2017). If the light response of stomatal opening is indeed mechanistically connected to the *PQ* redox state, the modified model may also provide a more generic parameterization across species, but more measurements on different species will be needed to assess this. However, although the species-specific differences between slope and intercept parameters as shown by Wolz et al. (2017) may have been aggravated by using A_n as an estimator of the stomatal light response, it is very likely that considerable species-specific parameterization will remain necessary in the modified model. For instance, whereas the blue-light response of guard cells is relatively weak in tobacco, which allowed lumping it in with the quantitative response in a single slope parameter $g_{1,new}$, this may possibly require more explicit parameterization in species with a stronger response to blue-light. The level of *NPQ* is also known to vary between species (Demmig-Adams 1998), within species (Jung and Niyogi 2009; Kasajima et al. 2011; Ortiz et al. 2017) and with leaf age and plant development stage (Bielczynski et al. 2017) and the same is true for photosynthetic capacity and leaf morphology. This is also evident from the model simulations of field-grown tobacco, where better fits could be obtained with substantially increased slope parameters (g_1, $g_{1,new}$) and decreased intercepts (g_0, $g_{0,new}$; Fig. 8 and Fig. S2). Different parameter values are to be expected based on known differences in stomatal acclimation between controlled and field conditions (Matthews et al. 2018). Late in the photoperiod, both models overestimated A_n and g_s. This may require more detail in the simulation of stomatal responses to vapour pressure deficit, leaf water status or long-term diurnal stomatal movements. For example, inclusion of a diurnal sinusoidal pattern in the BWB stomatal conductance model greatly improved prediction accuracy (Matthews et al. 2018). The physiological basis for these diurnal stomatal movements is not entirely clear, but circadian regulation (Hassidim et al. 2017) and interactions with sugar and ethylene signals (Kelly et al. 2013; Haydon et al. 2017) are well-known to have an impact on stomatal conductance. It is also clear that $1 - q_L$ will be subject to much faster changes than stomatal responses which suggests that the slower stomatal responses may reflect a time-averaged redox signal initiated at the chloroplastic PQ pool. Interestingly, the use of $1 - q_L$ in the stomatal conductance model would also allow the kinetic behavior of *NPQ* to impact stomatal dynamic properties, similar to our findings for steady state values (Głowacka et

al. 2018). Namely, build-up of sustained *NPQ* throughout the photo-period would directly dampen the signal for stomata to open in response to light. Further work is needed to test the relationship between *PQ* redox state and red light induced stomatal movements. The presented model equations provide a structured framework to generate and verify hypotheses based on this putative relationship.

Acknowledgements

We would like to thank David Drag and Ben Harbaugh for plant management in greenhouse and field studies, Liana Acevedo-Siaca for help with the diurnal gas exchange measurements and Nerea Ubierna and three anonymous reviewers for helpful comments on a previous version of the manuscript.

Compliance with ethical standards

This work was supported by the research project Realizing Increased Photosynthetic Efficiency (RIPE) that is funded by the Bill & Melinda Gates Foundation, Foundation for Food and Agriculture Research, and the Department for International Development under grant number OPP1172157. The authors declare that they have no conflict of interest.

References

Assman SM, Shimazaki K (1999) The Multisensory Guard Cell. Stomatal Responses to Blue Light and Abscisic Acid. Plant Physiology 119:809-815

Ball JT, Woodrow IE, Berry JA A Model Predicting Stomatal Conductance and its Contribution to the Control of Photosynthesis Under Different Environmental Conditions. In: Biggins J (ed) Progress in Photosynthesis Research, Providence, Rhode Island, USA, 1986. Springer Science, pp 221-224

Baroli I, Price GD, Badger MR, Von Caemmerer S (2008) The contribution of photosynthesis to the red light response of stomatal conductance. Plant Physiology 146:737-747

Bellasio C, Quirk J, Buckley TN, Beerling DJ (2017) A Dynamic Hydro-Mechanical and Biochemical Model of Stomatal Conductance for C4 Photosynthesis. Plant Physiology 175:104-119

Bielczynski LW, Lacki MK, Hoefnagels I, Gambin A, Croce R (2017) Leaf and Plant Age Affect Photosynthetic Performance and Photoprotective Capacity. Plant Physiology 175:1634-1648

Bilger W, Bjorkman O (1994) Relationships among violaxanthin deepoxidation, thylakoid membrane conformation, and nonphotochemical chlorophyll fluorescnece quenching in leaves of cotton (Gossypium hirsutum L.) Planta 193:238-246

Bonan GB, Williams M, Fisher RA, Oleson KW (2014) Modeling stomatal conductance in the earth system: linking leaf water-use efficiency and water transport along the soil-plant-atmosphere continuum. Geoscientific Model Development 7:2193-2222

Buckley TN (2017) Modeling Stomatal Conductance. Plant Physiology 174:572-582

Busch FA (2014) Opinion: The red-light response of stomatal movement is sensed by the redox state of the photosynthetic electron transport chain. Photosynthesis Research 119:131-140

Chater CCC, Caine RS, Fleming AJ, Gray JE (2017) Origins and Evolution of Stomatal Development. Plant Physiology 174:624-638

Damour G, Simonneau T, Cochard H, Urban L (2010) An overview of models of stomatal conductance at the leaf level. Plant Cell and Environment 33:1419-1438

Demmig-Adams B (1998) Survey of Thermal Energy Dissipation and Pigment Composition in Sun and Shade Leaves. Plant Cell Physiology 39:474-482

Dougherty RL, Bradford JA, Coyne PI, Sims PL (1994) Applying an empirical model of stomatal conductance to three C4 grasses Agricultural and Forest Meteorology 67:269-290

Engineer CB et al. (2016) CO2 Sensing and CO2 Regulation of Stomatal Conductance: Advances and Open Questions Trends in Plant Science 21:16-30

Evans J, Von Caemmerer S (2013) Temperature response of carbon isotope discrimination and mesophyll conductance in tobacco Plant Cell and Environment 36:745-756

Farquhar GD, Von Caemmerer S, Berry JA (1980) A biochemical model of photosynthetic CO2 assimilation in leaves of C3 species. Planta 149:78-90

Gamon JA, Penuelas J, Field CB (1992) A narrow-waveband spectral index that tracks diurnal changes in phoyosynthetic efficiency. Remote Sensing of Environment 41:35-44

Gamon JA, Serrano L, Surfus JS (1997) The photochemical reflectance index: an optical indicator of photosynthetic radiation-use efficiency across species, functional types, and nutrient levels. Oecologia 112:492-501

Genty B, Briantais JM, Baker NR (1989) The relationship between the quantum yield of photosynthetic electron transport and photochemical quenching of chlorophyll fluorescence. Biochimica et Biophysica Acta 990:87-92

Głowacka K et al. (2018) Photosystem II Subunit S overexpression increases the efficiency of water use in a field-grown crop. Nature communications 9:868

Gutschick VP, Simonneau T (2002) Modelling stomatal conductance of field-grown sunflower under varying soil water content and leaf environment: comparison of three models of stomatal response to leaf environment and coupling with an abscisic acid-based model of stomatal response to soil drying. Plant Cell and Environment 25:1423-1434

Hassidim M et al. (2017) CIRCADIAN CLOCK ASSOCIATED1 (CCA1) and the Circadian Control of Stomatal Aperture. Plant Physiology 175:1864-1877
Haydon MJ, O. M, Frank A, Roman A, Webb AAR (2017) Sucrose and Ethylene Signaling Interact to Modulate the Circadian Clock. Plant Physiology 175:947-958
Hendrickson L, Forster B, Pogson BJ, Chow WS (2005) A simple chlorophyll fluorescence parameter that correlates with the rate coefficient of photoinactivation of Photosystem II. Photosynthesis Research 84:43-49
Hilker T et al. (2011) Inferring terrestrial photosynthetic light use efficiency of temperate ecosystems from space. Journal of Geophysical Research 116:1-11
Inoue S, Kinoshita T (2017) Blue Light Regulation of Stomatal Opening and the Plasma Membrane H+-ATPase Plant Physiology 174:531-538
Johnson MP, Perez-Bueno ML, Zia A, Horton P, Ruban AV (2009) The Zeaxanthin-Independent and Zeaxanthin-Dependent qE Components of Nonphotochemical Quenching Involve Common Conformational Changes within the Photosystem II Antenna in Arabidopsis. Plant Physiology 149:1061-1075
Jung H-S, Niyogi KK (2009) Quantitative Genetic Analysis of Thermal Dissipation in Arabidopsis. Plant Physiology 150:977-986
Kaiser H, Kappen L (1997) In situ observations of stomatal movements in different light-dark regimes: the influence of endogenous rhythmicity and long-term adjustments. Journal of Experimental Botany 48:1583-1589
Kasajima I, Ebana K, Yamamoto T, Takahara K, Yano M, Kawai-Yamada M, Uchimiya H (2011) Molecular distinction in genetic regulation of nonphotochemical quenching in rice. Proceedings of the National Academy of Sciences 108:13835-13840
Kelly G et al. (2013) Hexokinase mediates stomatal closure The Plant Journal 75:977-988
Kollist H, Nuhkat M, Roelfsema MRG (2014) Closing gaps: linking elements that control stomatal movement. New Phytologist 203:44-62
Kramer DM, Johnson G, Kiirats O, Edwards GE (2004) New fluorescence parameters for the determination of QA redox state and excitation energy fluxes Photosynthesis Research 79:209-218
Kromdijk J, Schepers H, Griffiths H (2010) Can the progressive increase of C4 bundle sheath leakiness at low PFD be explained by incomplete suppression of photorespiration? Plant Cell and Environment 33:1935-1948
Lawson T, Lefebvre S, Baker NR, Morison JI, Raines CA (2008) Reductions in mesophyll and guard cell photosynthesis impact on the control of stomatal responses to light and CO2. Journal of Experimental Botany 59:3609-3619
Lawson T, Simkin AJ, Kelly G, Granot D (2014) Mesophyll photosynthesis and guard cell metabolism impacts on stomatal behaviour. New Phytologist 203:1064-1081
Leuning R (1995) A critical appraisal of a combined stomatal-photosynthesis model for C3 plants Plant Cell and Environment 18:339-355
Liang YK, Dubos C, Dodd IC, Holroyd GH, Hetherington AM, Campbell MM (2005) AtMYB61, an R2R3-MYB Transcription Factor Controlling Stomatal Aperture in Arabidopsis thaliana. Current Biology 15:1201-1206
Loriaux SD, Avenson TJ, Welles JM, McDermitt DK, Eckles RD, Riensche B, Genty B (2013) Closing in on maximum yield of chlorophyll fluorescence using a single multiphase flash of sub-saturating intensity Plant Cell and Environment 36:1755-1770
Marten H, Hyun T, Gomi K, Seo S, Hedrich R, Roelfsema MRG (2008) Silencing of NtMPK4 impairs CO2-induced stomatal closure, activation of anion channels and cytosolic Ca2+ signals in Nicotiana tabacum guard cells. The Plant Journal 55:698-708
Matthews JSA, Vialet-Chabrand SRM, Lawson T (2018) Acclimation to Fluctuating Light Impacts the Rapidity of Response and Diurnal Rhythm of Stomatal Conductance. Plant Physiology 176:1939-1951

Medlyn B et al. (2011) Reconciling the optimal and empirical approaches to modelling stomatal conductance. Global Change Biology 17:2134-2144
Messinger SM, Buckley TN, Mott KA (2006) Evidence for Involvement of Photosynthetic Processes in the Stomatal Response to CO2 Plant Physiology 140:771-778
Mielke MS, Oliva MA, De Barros NF, Penchel RM, Martinez CA, De Almeida AC (1999) Stomatal control of transpiration in the canopy of a clonal Eucalyptus grandis plantation. Trees 13:152-160
Morales A, Yin X-Y, Harbinson J, Driever SM, Kramer DM, Struik PC (2018) In silico analysis of the regulation of the photosynthetic electron transport chain in C3 plants. Plant Physiology 176:1247-1261
Mott KA, Parkhurst DF (1991) Stomatal responses to humidity in air and helox. Plant Cell and Environment 14:509-515
Mott KA, Sibbernsen ED, Shope JC (2008) The role of the mesophyll in stomatal responses to light and CO2 Plant Cell and Environment 31:1299-1306
Ortiz D, Hu J, Fernandez MGS (2017) Genetic architecture of photosynthesis in Sorghum bicolor under non-stress and cold stress conditions. Journal of Experimental Botany 68:4545-4557
Oxborough K, Baker NR (1997) Resolving chlorophyll a fluorescence images of photosynthetic efficiency into photochemical and non-photochemical components – calculation of qP and Fv'/Fm' without measuring Fo' Photosynthesis Research 54:135-142
Pearcy RW, Schulze E-D, Zimmermann R (1989) Measurement of transpiration and leaf conductance. In: Pearcy RW, Ehleringer JR, Mooney HA, Rundel PW (eds) Plant Physiological Ecology - Field methods and instrumentation. Chapman and Hall, London, pp 137-153
Porcar-Castell A et al. (2014) Linking chlorophyll a fluorescence to photosynthesis for remote sensing applications: mechanisms and challenges. Journal of Experimental Botany 65:4065-4095
Sharkey TD, Bernacchi CJ, Farquhar GD, Singsaas EL (2007) Fitting photosynthetic carbon dioxide response curves for C3 leaves. Plant Cell and Environment 30:1035-1040
Tenhunen JD, Sala A, Harley PC, Dougherty RL, Reynolds JF (1990) Factors influencing carbon fixation and water use by Mediterranean sclerophyll shrubs during summer drought. Oecologia 82:381-393
Vialet-Chabrand SRM, Matthews JSA, McAusland L, Blatt MR, Griffiths H, Lawson T (2017) Temporal Dynamics of Stomatal Behavior: Modelling and Implications for Photosynthesis and Water Use. Plant Physiology 174:603-613
Von Caemmerer S, Lawson T, Oxborough K, Baker NR, Andrews TJ, Raines CA (2004) Stomatal conductance does not correlate with photosynthetic capacity in transgenic tobacco with reduced amounts of Rubisco. Journal of Experimental Botany 55
Wang F-F, Lian H-L, Kang C-Y, Yang H-Q (2010) Phytochrome B is Involved in Mediating Red Light-Induced Stomatal Opening in Arabidopsis thaliana. Molecular Plant 3:246-259
Wang Y et al. (2017) Unexpected Connections between Humidity and Ion Transport Discovered Using a Model to Bridge Guard Cell-to-Leaf Scales. The Plant Cell 29:2921-2939
Wang YP, Leuning R (1998) A two-leaf model for canopy conductance, photosynthesis and partitioning of available energy I. Model description and comparison with a multi-layered model. Agricultural and Forest Meteorology 91:89-111
Wehr R et al. (2017) Dynamics of canopy stomatal conductance, transpiration, and evaporation in a temperate deciduous forest, validated by carbonyl sulfide uptake. Biogeosciences 14:389-401
Wei Z, Yoshimura K, Wang L, Miralles DG, Jasecko S, Lee X (2017) Revisiting the contribution of transpiration to global terrestrial evapotranspiration. Geophysical Research Letters 44:2792-2801
Whitehead D (1998) Regulation of stomatal conductance and transpiration in forest canopies. Tree Physiology 18:633-644
Wolz KJ, Wertin TM, Abordo M, Wang D, Leakey A (2017) Diversity in stomatal function is integral to modelling plant carbon and water fluxes Nature ecology and evolution 1:1292-1298
Yin X-Y, Struik PC, Romero P, Harbinson J, Evers JB, Van der Putten PEL, Vos J (2009) Using combined measurements of gas exchange and chlorophyll fluorescence to estimate parameters of

a biochemical C3 photosynthesis model: a critical appraisal and a new integrated approach applied to leaves in a wheat (Triticum aestivum) canopy. Plant Cell and Environment 32:448-464

Zaks J, Amarnath K, Kramer DM, Niyogi KK, Fleming GR (2012) A kinetic model of rapidly reversibly nonphotochemical quenching. Proceedings of the National Academy of Sciences 109:15757-15762

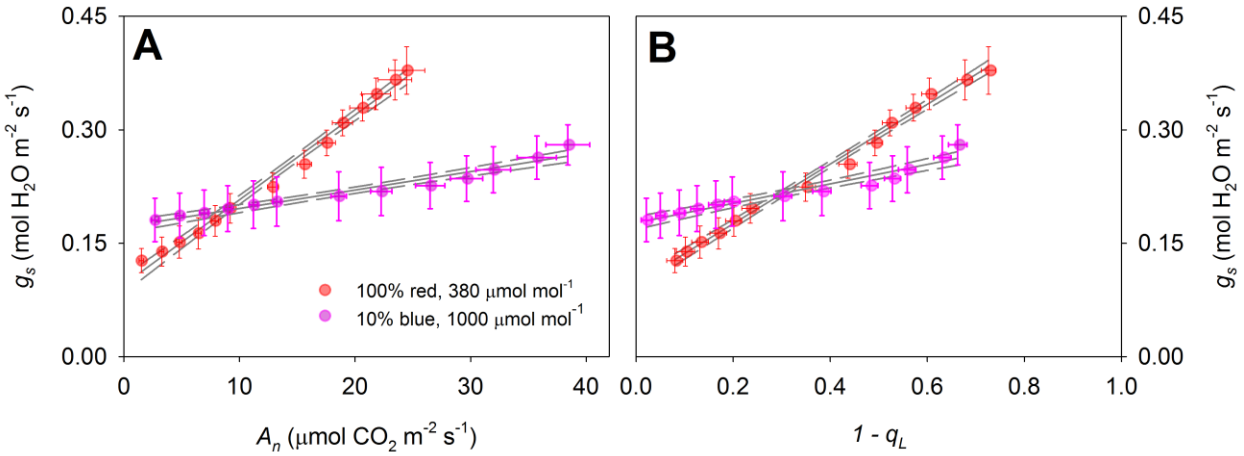

Fig. 1 (A) Stomatal conductance (g_s) plotted as a function of net assimilation rate (A_n). (B) Stomatal conductance plotted as a function of fluorescence parameter $1\text{-}q_L$. Red symbols indicate measurements performed at CO_2 concentration in the cuvette of 380 µmol mol^{-1}, 100% red light, purple symbols indicate measurements at CO_2 of 1000 µmol mol^{-1}, 90% red 10% and blue light. Solid and dashed lines show linear regressions and 95% confidence intervals, respectively. Error bars indicate standard errors (n = 6-7 biological replicates).

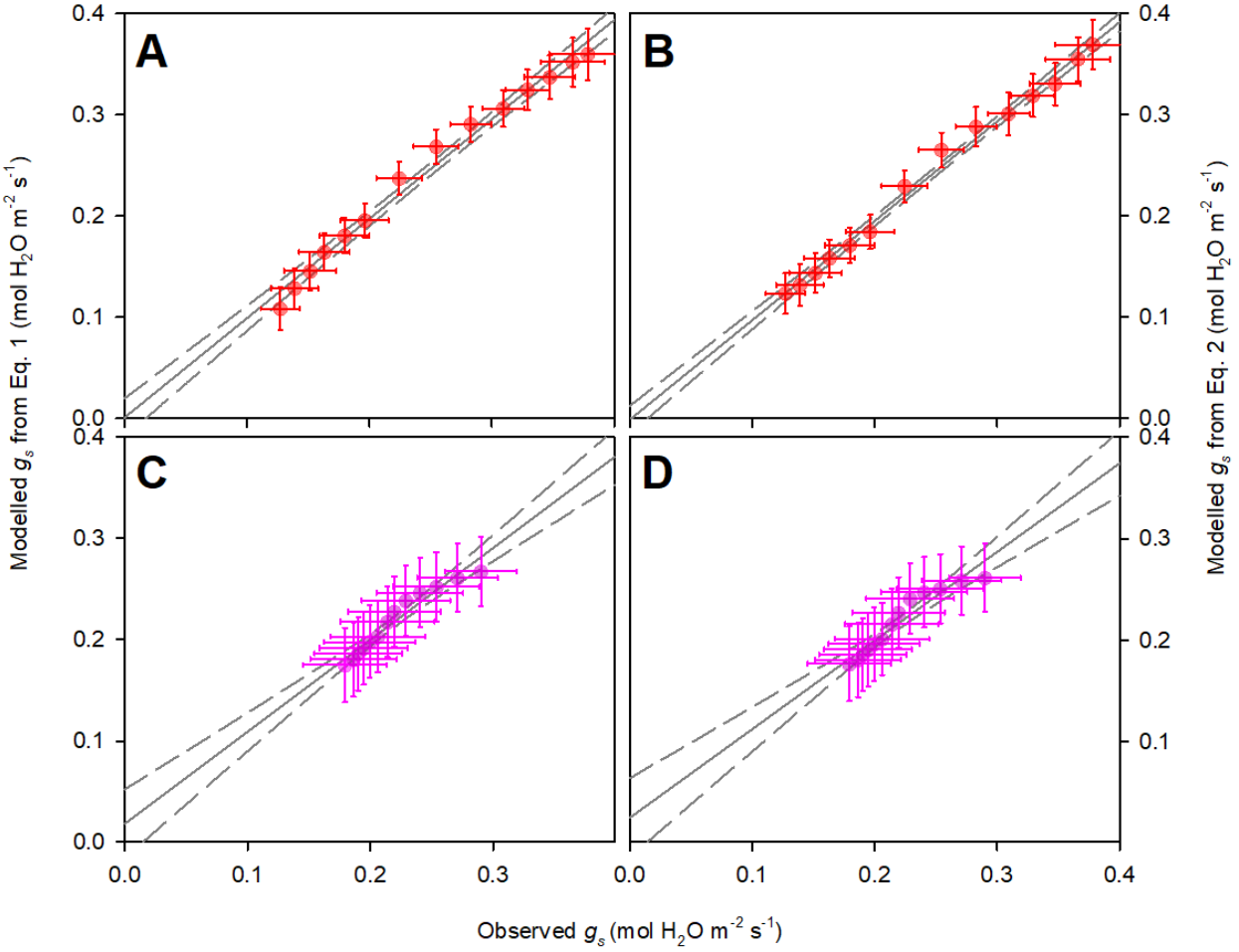

Fig. 2 Measured versus modelled stomatal conductance (g_s). Stomatal conductance was modelled for measurements performed at CO_2 concentration in the cuvette of 380 µmol mol^{-1} and 100% red light with Eq. 1 (Medlyn *et al.* 2011, panel A) and with the modified model (Eq. 2, panel B) and for measurements using 90% red and 10% blue light and CO_2 of 1000 µmol mol^{-1} with the Medlyn model (panel C) and with the modified model (panel D). Solid and dashed lines show linear regressions and 95% confidence intervals, respectively. Error bars indicate standard errors (n = 6 biological replicates).

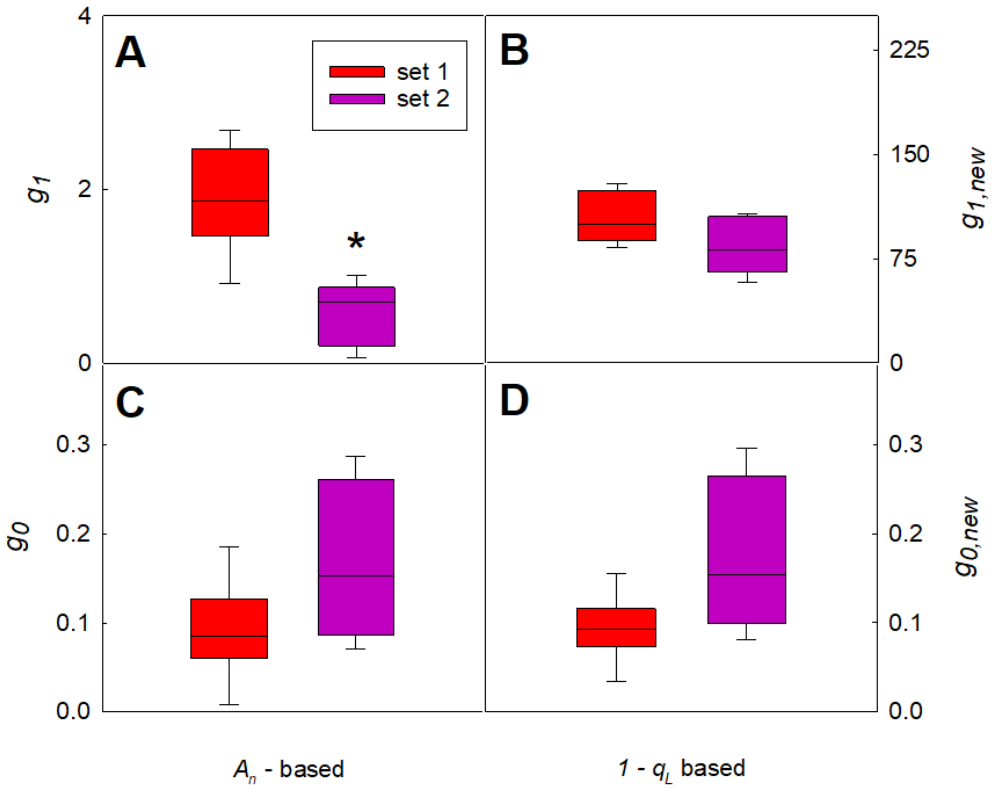

Fig. 3 Estimated model parameters (g_0, $g_{0,new}$, g_1, $g_{1,new}$)) for the stomatal conductance model with either A_n (panel A and C) or $1 - q_L$ (panel B and D) as the estimator for light-induced stomatal movements. Light response curves were measured with either 100% red light and 380 µmol mol^{-1} CO_2 (set 1) or 90% red and 10% blue light and 1000 µmol mol^{-1} CO_2 (set 2). Asterisk indicates significant difference between parameter estimate for set 1 versus set 2 (P = 0.001, Student's t-test, n = 6).

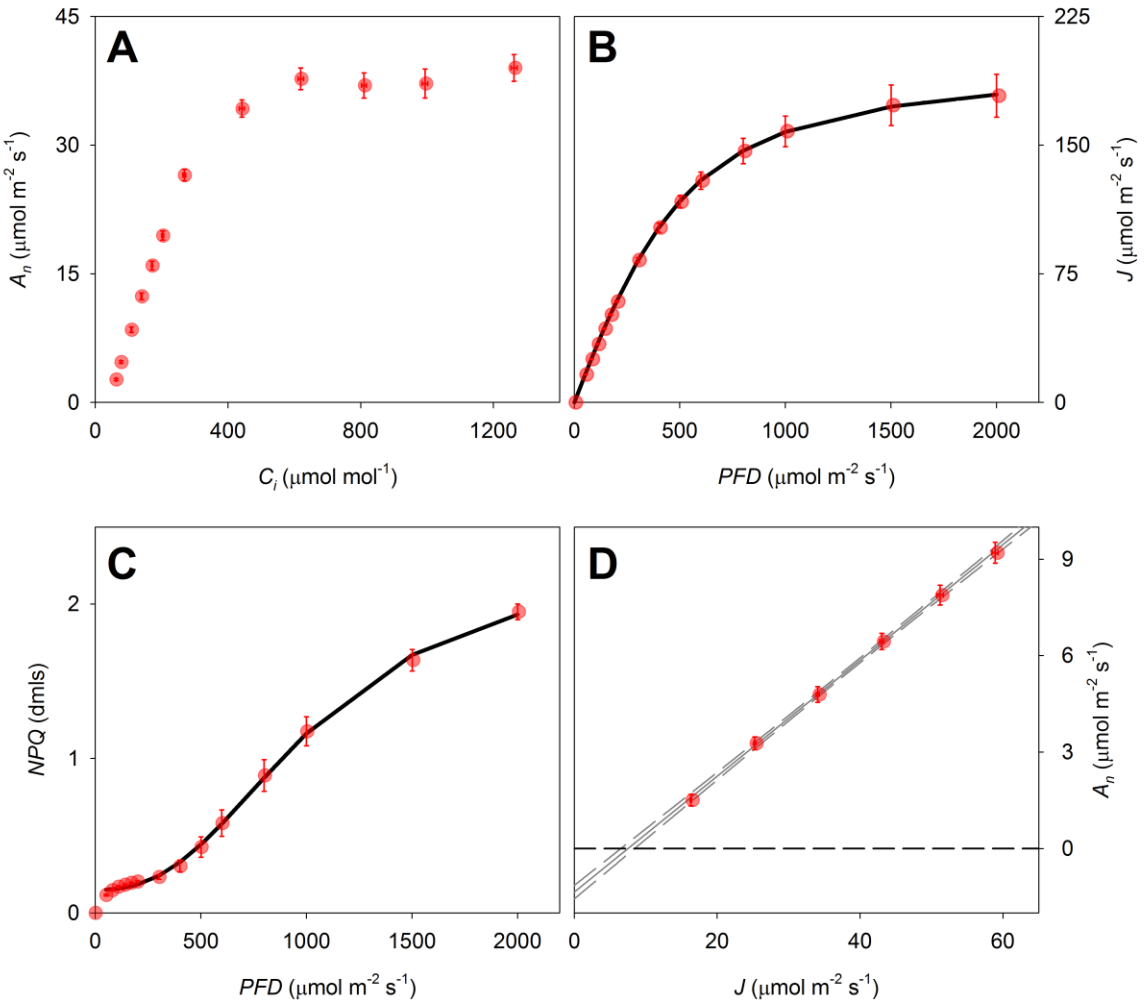

Fig. 4 Response curves to derive model parameters for the photosynthesis model. Net assimilation rate A_n plotted as a function of (A) intercellular CO_2 concentration (C_i), (B) whole-chain electron transport (J) and (C) non-photochemical quenching (NPQ) plotted as a function of incident light (PFD) and (D) A_n plotted as a function of J. Solid lines in B and C depict model fits (Eq. 11 and 13). The data in D was used to estimate mitochondrial respiration rate not associated with photorespiration (R_d) as the y-intercept of the linear correlation. Solid and dashed lines in (D) show linear regressions and 95% confidence intervals, respectively. Error bars indicate standard errors (n = 6 biological replicates).

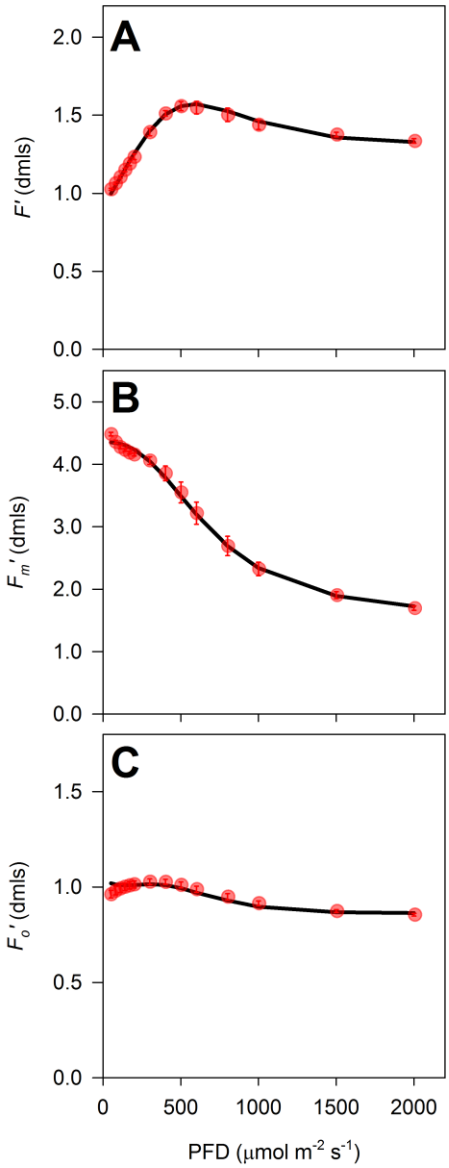

Fig. 5 (A) Steady state fluorescence (*F*'), (B) maximal fluorescence under illumination (F_m') and (C) minimal fluorescence under illumination (F_o'). Symbols indicate measurements (scaled to corresponding F_m measurement), solid lines show model simulations. Error bars indicate standard errors (n = 6 biological replicates).

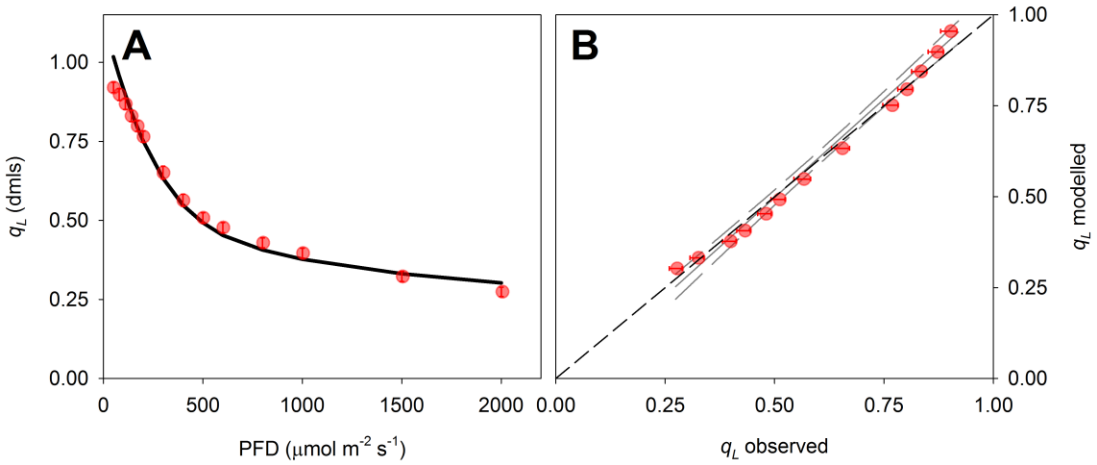

Fig. 6 (A) Fluorescence parameter q_L as a function of light intensity (PFD), symbols indicate measurements, solid line shows modelled. (B) Correlation between observed and modelled q_L shown in panel A. Solid and dashed lines in B depict linear regression (y = 1.08x - 0.04) and 95% confidence intervals, respectively. Slope and intercept did not deviate significantly from x = y shown by the black dashed line (P > 0.05). Error bars indicate standard errors (n = 6 biological replicates).

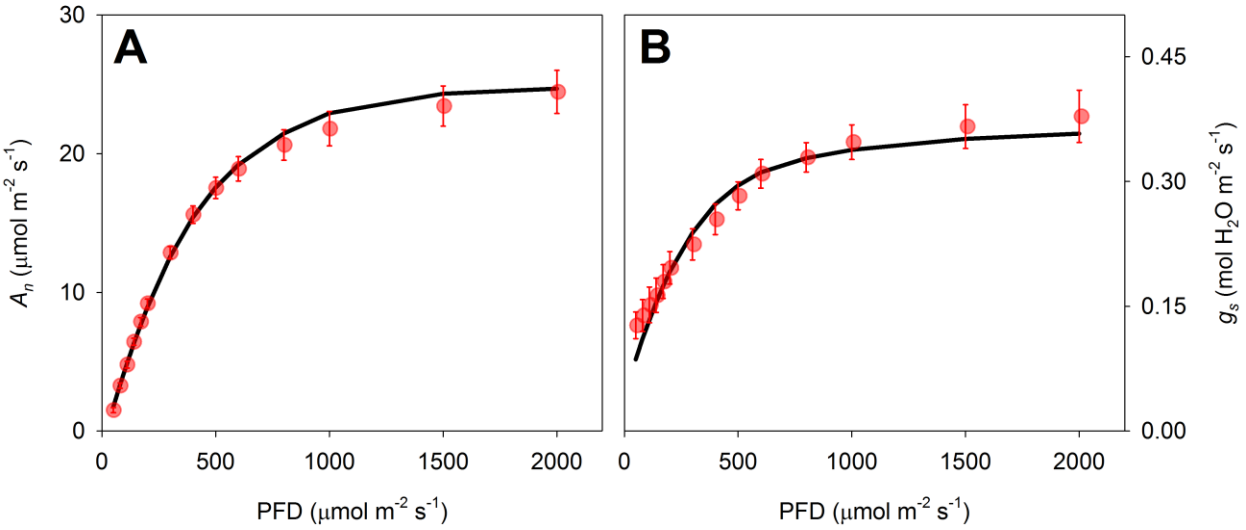

Fig. 7 Observed and modelled A_n (A) and g_s (B) as a function of light intensity. Model simulations were performed with the coupled model for photosynthesis and stomatal conductance. Error bars indicate standard errors (n = 6 biological replicates).

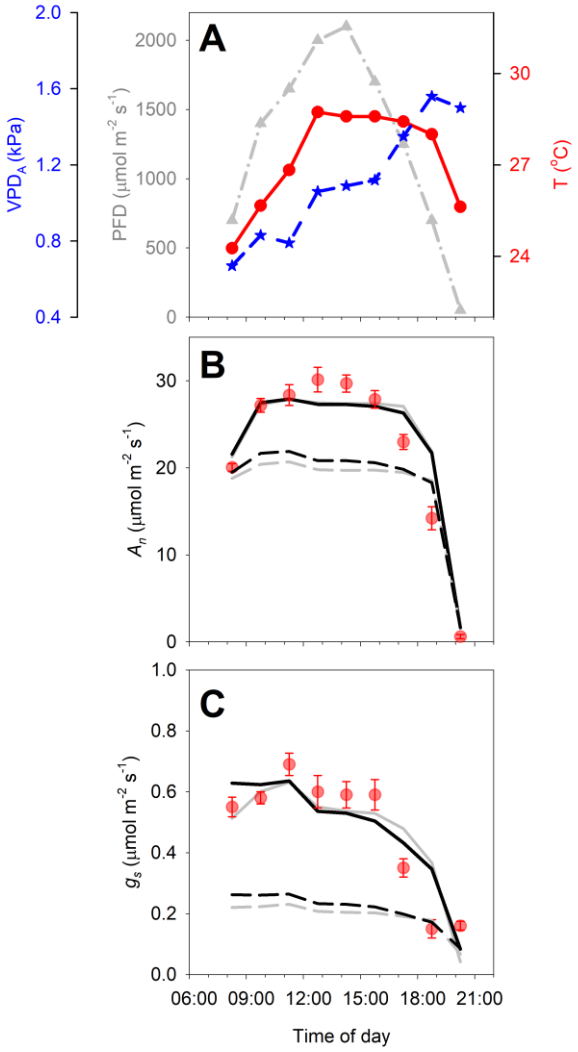

Fig. 8 (A) Diurnal measurements of light intensity (PFD), air temperature (T) and air vapour pressure deficit (VPD_A) during July 21, 2015 in Urbana, Illinois, USA. (B) Observed (symbols) and modelled (lines) net assimilation rate (A_n) at 90 min intervals. Simulations were performed with the coupled photosynthesis-stomatal conductance model, using the weather data in (A) as input. Lines show model predictions using either the Medlyn (grey lines) or the modified stomatal conductance model (black lines), with parameter estimates from controlled conditions (dotted lines) or re-calibrated on field-grown plants (solid lines) (C) Observed (symbols) and modelled (lines) stomatal conductance (g_s). Line legend as explained for (B). Error bars indicate standard errors (n = 7-8 biological replicates).

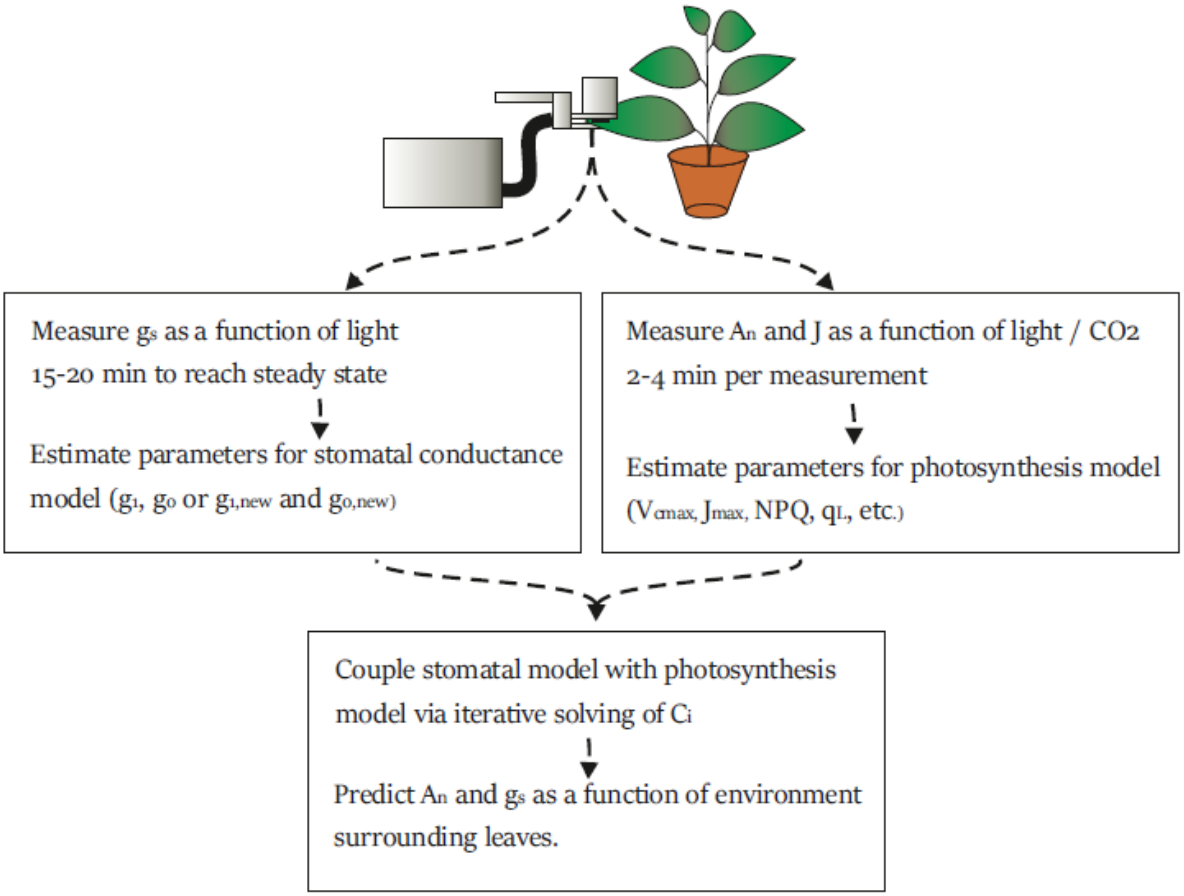

Fig. S1 Schematic of measurements and model parameterization.

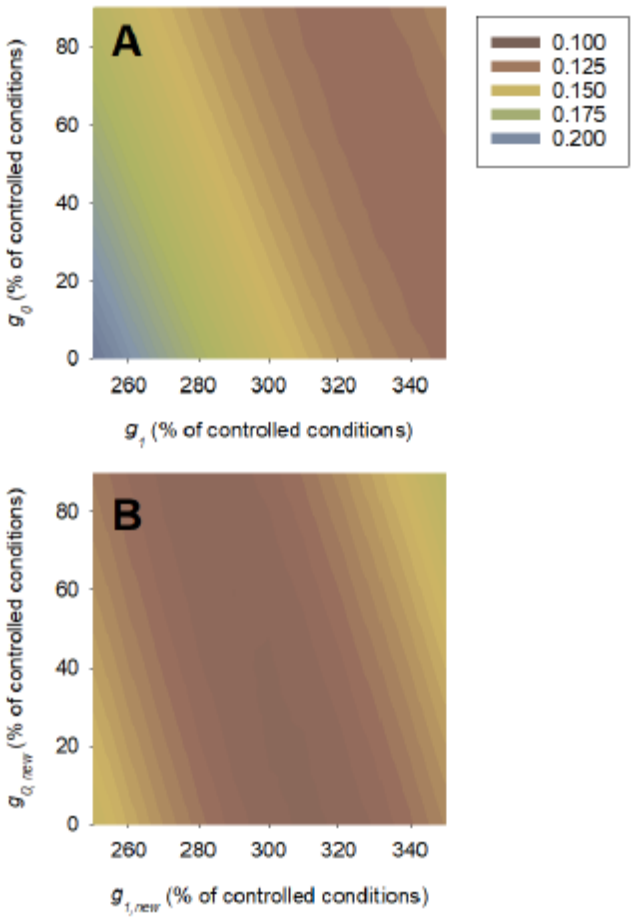

Fig. S2 Residuals for modelled compared to observed stomatal conductance (g_s) under field conditions shown in Fig. 8A. (A) Residuals for predictions with the Medlyn stomatal conductance model coupled to the photosynthesis model at a wide range of values for g_0 and g_1 (depicted as percentage of the values for controlled-conditions grown plants). (B) Same as (A) but for the modified model. Legend shows color-coding for residuals.

Table 1 Model parameter estimates under controlled and field conditions

Parameter name	Description	Unit	Greenhouse (Value at 25 ºC)	Field (Value at 25 ºC)	Source
g_0	Intercept parameter in Medlyn stomatal conductance model.	mol H_2O m^{-2} s^{-1}	0.091	0.027	Eq.1 fit on light response curves (controlled conditions) or combined photosynthesis-stomatal conductance model fit on diurnal data (field).
g_1	Slope parameter in Medlyn stomatal conductance model.	Dimensionless	1.90	6.46	Eq.1 fit on light response curves (controlled conditions) or combined photosynthesis-stomatal conductance model fit on diurnal data (field).
$g_{0,new}$	Intercept parameter in modified stomatal conductance model.	mol H_2O m^{-2} s^{-1}	0.093	0	Eq.2 fit on light response curves (controlled conditions) or combined photosynthesis-stomatal conductance model fit on diurnal data (field).
$g_{1,new}$	Slope parameter in modified stomatal conductance model.	Dimensionless	104	322	Eq.2 fit on light response curves (controlled conditions) or combined photosynthesis-stomatal conductance model fit on diurnal data (field).
V_{cmax}	Maximal rate of RuBP carboxylation.	µmol m^{-2} s^{-1}	121	115.2	Fitted on CO_2 response curves.
V_{TPU}	Maximal rate of triose phosphate utilization.	µmol m^{-2} s^{-1}	11.5	14.1	Fitted on CO_2 response curves.
g_m	Mesophyll conductance to CO_2 transfer.	mol CO_2 m^{-2} s^{-1} bar^{-1}	0.60	0.60	Derived from carbon isotope measurements
R_d	Mitochondrial respiration not associated with photorespiration, under illuminated conditions.	µmol m^{-2} s^{-1}	1.35	1.16	Estimated as y-intercept of linear correlation between A_n vs J under light limited range.
J_{max}	Maximal rate of whole-chain electron transport (J).	µmol m^{-2} s^{-1}	205	200	Estimated from fitting non-rectangular hyperbole to chlorophyll fluorescence measurements during light response curves.
α	Initial slope non-rectangular	Electrons / photons	0.79	0.72	Estimated from fitting non-rectangular hyperbole to

	hyperbolic fit of *J* response to light intensity.				chlorophyll fluorescence measurements during light response curves.
θ	Shape factor non-rectangular hyperbolic fit of *J* response to light intensity.	Dimensionless	0.74	0.75	Estimated from fitting non-rectangular hyperbole to chlorophyll fluorescence measurements during light response curves.
f_{PSII}	Proportion of absorbed light partitioned to PSII	Dimensionless	0.50	0.50	Not estimated here.
NPQ_{max}	Asymptote value sigmoidal fit of non-photochemical quenching (*NPQ*) response to light intensity.	Dimensionless	2.24	2.81	Estimated from fitting sigmoidal Hill function to chlorophyll fluorescence measurements during light response curves.
NPQ_0	Basal *NPQ* value	Dimensionless	0.15	0.42	Estimated from fitting sigmoidal Hill function to chlorophyll fluorescence measurements during light response curves
K_{NPQ}	Light intensity at half amplitude of *NPQ*.	Dimensionless	1042	1672	Estimated from fitting sigmoidal Hill function to chlorophyll fluorescence measurements during light response curves
n_{NPQ}	Apparent Hill coefficient for NPQ response to light.	Dimensionless	2.52	2.28	Estimated from fitting sigmoidal Hill function to chlorophyll fluorescence measurements during light response curves
m	Slope parameter to estimate effect of reaction center inactivation on minimal fluorescence (F_o').	Dimensionless	2.34×10^{-4}	2.34×10^{-4}	Estimated from fitting Eq. 17 on chlorophyll fluorescence measurements during light response curves.
n	Intercept parameter to estimate effect of reaction center inactivation on F_o'.	Dimensionless	0.038	0.038	Estimated from fitting Eq. 17 on chlorophyll fluorescence measurements during light response curves.